

Water drop impact on thin viscous oil layers

Surjit Bharatsingh[†], Piyush Sahu[†], Gaurav Salwan and Dileep Mampallil*

Indian Institute of Science Education & Research Tirupati,

Yerpedu P. O. PIN 517619, Tirupati, AP, INDIA

(Dated: July 19, 2024)

We conducted experimental investigations into the short-term and long-term impact dynamics of pure water drops on silicone oil-coated surfaces. Our observations revealed distinct phases: initially, rapid maximal spreading followed by retraction, subsequent oscillations characterized by a relatively stable contact angle, and a final phase involved the gradual spreading of the drop on the underlying solid surface due to the rupturing of the oil layer. The maximal spreading radius follows $We^{1/4}$ scaling, where We is the Weber number, independent of the viscosity of the underlying oil layer. By introducing fluorescent tracer particles in the oil, we noted that the drop expanded over the oil layer during the initial spreading without displacing oil. Subsequently, as the oscillations dampen, the drop ruptures the oil layer, initiating a dewetting process and spreads over the solid surface, leaving a tiny oil droplet under the water drop. Upon completion of this dewetting process, the onset time for the drop spreading nonlinearly increased with the oil layer thickness as $\sim d_o^2$, which we attribute to the dewetting dynamics. Our findings unveil intriguing dynamics of water drops impacting on oil-coated surfaces.

Keywords: Drop impact, oil film

[†] Equal contribution

INTRODUCTION

Fundamental understanding of drop impact [1–5] on various surfaces such as pre-wetted [4], superhydrophobic [6], granular [7, 8] and liquid [1, 9] surfaces and subsequent spreading [10] has implications in various fields such as inkjet printing [11], drop-impact printing [12], cooling systems [13], spraying of pesticides and medicines [14], to list a few. These applications also involve the impact of drops of complex fluids [15, 16], such as blood drops, where the resulting patterns have implications in forensics [16, 17]. Thus, understanding the fundamental dynamics of drop impact is important in many processes.

The dynamics of a liquid drop after impacting a surface depends upon the drop size, impact velocities, properties of the liquid, and the physical nature of surface, such as wettability and roughness [2, 3, 5]. The impact dynamics demonstrate spreading, rebounding, splashing, and break-up depending upon the liquid and surface properties and impact energies [2, 3]. Upon impact, the inertia expands the liquid on the surface, which is balanced by viscous and surface tension forces [18, 19]. Drop impact on hydrophobic and superhydrophobic surfaces [6, 20] shows bouncing of the drop with a short contact time that depends upon the inertia, surface tension, and liquid-surface interactions [21, 22]. Relative temperature difference between the impacting liquid and the solid can also lead to non-sticking effects [23]. The ambient medium (usually air) also influences drop impact dynamics on solid surfaces. The local increase in pressure between the impacting face of the drop and substrate surface deforms the impacting face, eventually entrapping a thin layer of air upon impact [24]. Drop impact on gran-

ular medium [25–27] can demonstrate the effects of this air entrapment as patterns on the granular layer and also microbubble generation [8].

Impact drops on soft and viscoelastic surfaces [28, 29], and even immiscible liquids [9], have also attracted scientific interest. The spreading and retraction of drops on soft surfaces strongly depend upon the viscoelastic properties of the surface [29, 30]. On such surfaces, the contact angle hysteresis can dissipate much of the impact energy, especially during retraction.

In the case of drop impact on liquid layers, the competition between the inertial, capillary, and viscous effects determines the dynamics after impact. An example is the water drop impact on oil layers [31] and oil-infused surfaces [32–34]. These studies show that impact energy and oil viscosity determines the dynamics of both the drop and the oil [31, 32]. Further, Lee et al. showed that the viscosity of the oil film does not have significant effect on the maximal spreading radius of impacted water drops [32]. However, at lower oil viscosity, the bouncing of the drop is enhanced [33]. The crown formation of the impacted drop also vivid at relatively higher impact velocities [31]. Previous studies indicate that the interaction between water drops impacting oil layers, or, more broadly, the impact of drops on liquid layers, is a complex process that requires further exploration.

In this research, we experimentally study water drop impacting a highly viscous silicone oil layer coated on various substrates and demonstrate several previously unreported dynamics. When the drop impacts, it rapidly spreads without disrupting the oil layer. However, during the subsequent retraction phase, the contact line drags the oil layer inward and thus the drop dissipates the impact energy. Additionally, the drop exhibits damping oscillations and slowly penetrates the oil layer. We find that the time the drop takes for this penetration increases with the oil layer thickness and impact velocity, contrary

to the expected rupturing the oil layer immediately upon impact. We systematically investigate the different dynamics exhibited by the impacted drop and draw comparisons with established scaling laws.

EXPERIMENTS

We spin-coated silicone oil on glass slides sequentially cleaned with isopropyl alcohol and water followed by air drying. The spin coating of silicone oil was performed at different rpm ranging 500 to 5000. Different rpm resulted in different thickness of the oil, depending upon the oil viscosity (μ_o), such as 370 and 10000 cSt (Sigma Aldrich). The oil thickness was obtained by comparing the weight of the glass slide in a microbalance (Quintix224-10IN) before and after the uniform coating with the oil. The thickness was obtained as $d_o = \delta m \rho_o A$, where δm is the oil mass, ρ_o is the density of oil, and A is the area of the glass slide. An average thickness was obtained from five different samples. The relationship between the spin rpm and the oil layer thickness for different oils are shown in Supplementary Fig.S1. We compared the measured oil thicknesses to the ones obtained using the Meyerhofer model [35], which gives the spin-coated thickness as $(3\mu_o/4\rho_o\omega^2T)^{1/2}$, where, ω is the angular velocity of spinning and T is the duration of the spinning. The calculated values were higher than the measured ones up to two times, especially at lower rpm. We used the experimental values of the thickness for further analyses.

We coated oil on different substrates such as, glass, indium tin oxide (ITO), and polydimethylsiloxane (PDMS). On these bare surfaces (without oil coat), water drops have contact angles of $22 \pm 2^\circ$, $60 \pm 2^\circ$. and $100 \pm 2^\circ$, respectively.

Water drops of volume $6.5 \mu\text{l}$ (with 5% deviation) having radius $R = 1.1 \text{ mm}$ was dropped from a Teflon tubing connected to a syringe pump. The impact height varied from 0 to 0.95 m. The corresponding impact velocity varied between 0 and 4.3 m/s. Upon impact, the dynamics of the drop was imaged using a high-speed camera (Phantom MICRO LAB110) at frame rates up to 5000. The images were analyzed using ImageJ software and home-made Matlab code to obtain the contact angle and base radius as a function of time.

RESULTS

To begin, we will provide an overview of the observations regarding the behavior of liquid drops impacting on oil-coated glass slides as shown in Fig.1. The dynamics of the drop's base radius and contact angle are quantified in Fig. 2(a) and 2(b), respectively. Upon impact,

the drop rapidly spreads to reach its maximum base diameter (D_{max}) in approximately 4 milliseconds. As the impact velocity increases, the time required to achieve maximum spreading becomes shorter (Fig.1). Just before the drop retracts, the contact angle decreases to a minimum value in proportion to the impact velocity. Subsequently, the drop enters a phase of retraction followed by damping oscillations while maintaining a relatively constant average contact angle of around 100 degrees in a quasi-equilibrium state. Notably, after about a second, the drop undergoes a slow spreading phase, indicated by an increase in the base radius and a decrease in the contact angle. We will delve into these features of the curves in Fig 2 in the subsequent discussions.

The maximum spreading diameter: Upon impact, in the absence of splash, the maximum spreading diameter [3, 18, 36–40] is an important parameter in several applications involving drop impact. The maximum spreading is characterized by a factor, β , which is the ratio of the diameter upon maximum spreading (D_{max}) to that at the initial spherical drop ($D = 2R$). The value of β results from the balance of kinetic energy, surface energy, and viscous dissipation. Considering these aspects, numerous relationships were derived connecting β to dimensionless numbers such as, Webber number, $We = \rho_w Du_i^2 / \sigma_w$ and Reynolds number, $Re = \rho_w Du_i / \mu_w$, where, ρ_w is the density of the impacting liquid (water), u_i is its impact velocity, σ_w is the surface tension, and μ_w is the viscosity of the impacting drop. In the viscous regime where spreading occurs by a balance between the kinetic energy and the viscous dissipation, $\beta \sim Re^{1/5}$ was reported [3, 37]. When viscous effects are small, a comparison of the initial kinetic energy with the capillary energy has predicted $\beta \sim We^{1/2}$ at asymptotic regimes of large Webber numbers. Clanet et al. derived another scaling law, $\beta \sim We^{1/4}$, considering the volume conservation between the initial spherical and the final pancake shapes [18]. They considered that the final thickness of the pancake drop is proportional to the capillary length $a_c = \sqrt{\sigma_w / (\rho_w g')}$, where $g' \sim u_i / D$ is an increased acceleration experienced by the drop during the spreading.

In our experiments, we observe the scaling $\beta \sim We^{1/4}$. Although the scaling $We^{1/4}$ was first demonstrated for low-viscosity drop impact on strongly water repellent surfaces [18], impact on various surfaces [3, 38] including oil-infused surfaces [32] have shown this scaling. Impact of viscous drops such as water-glycerol (6 & 51 cSt) and blood drops on steel surfaces have also shown $We^{1/4}$ scaling [40]. Various other works reported different scaling

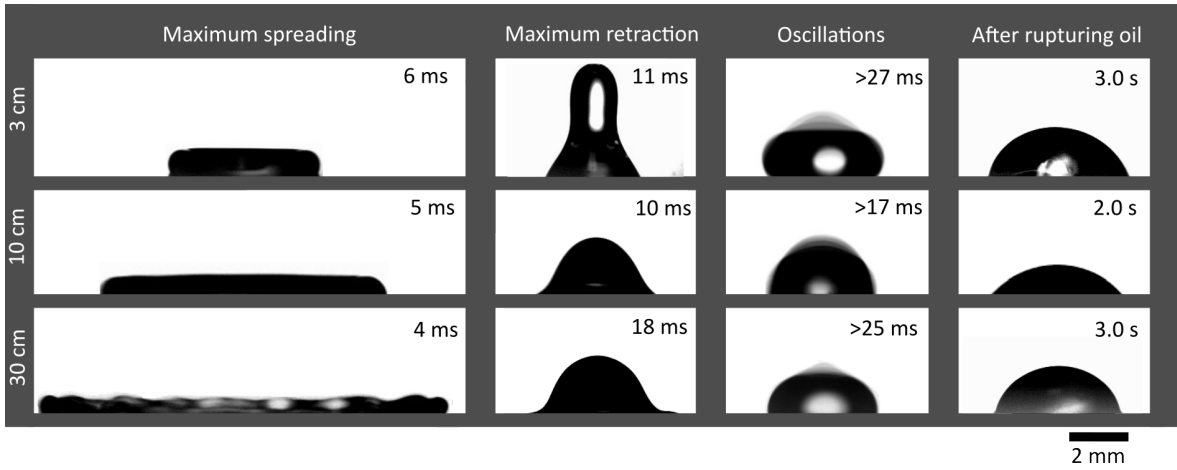


Figure 1. Impact dynamics of water drops dispensed from three different heights (3, 10, 30 cm) onto silicon oil layer of thickness $7 \mu\text{m}$. The oil viscosity was 370 cSt. From the video recorded at 2000 fps, the images corresponding to different regimes are shown. The oscillation phase continues to several hundreds of milliseconds. During this process the drop edge penetrates into the oil layer. This aspect is characterized by the spreading of the drop as it meets the underlying hydrophilic surface (glass).

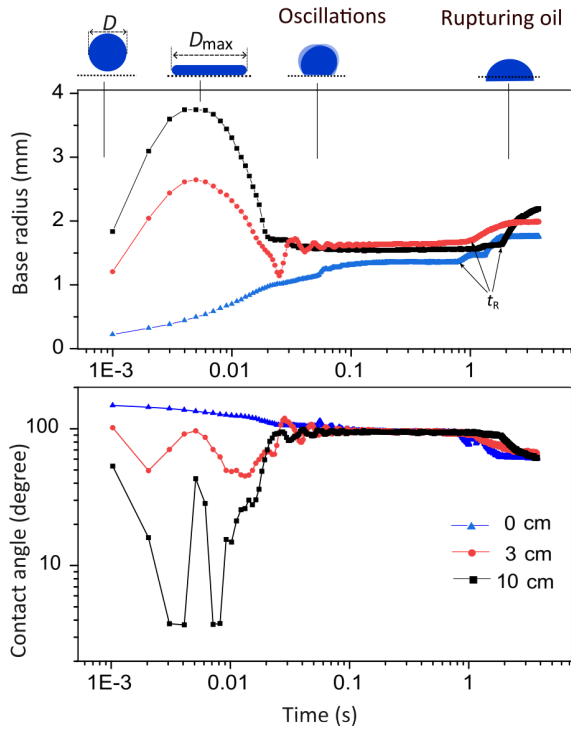


Figure 2. The base radius and contact angle of drops placed softly and impacted from two different heights (3 and 10 cm) onto silicon oil layer of thickness $7 \mu\text{m}$ coated on glass. The oil viscosity was 370 cSt. Upon maximum spread, the contact angle decreases to a minimum and the contact line is dragged on the oil layer during the retraction. With increasing impact height, the energy loss during the dragging phase increases resulting in a weak oscillation phase. The drop spreads on the surface at $t = t_R$, when the contact line meets the substrate, manifested by a decrease in the contact angle.

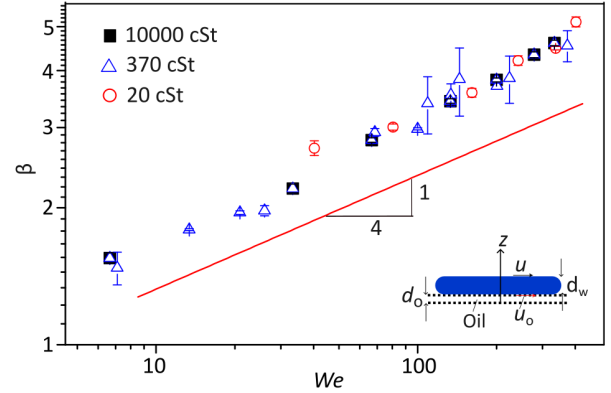


Figure 3. The maximum spreading parameter β as a function of Weber number. The error bars are the standard deviation from at least five measurements. The inset illustrates a drop spreading on the oil layer with various parameters marked.

laws as $We^{1/2}$, $We^{1/4}$, $Re^{1/4}$, $Re^{1/5}$ or complex relationships suggesting a universal scaling [3, 40, 42]. Since correlating the scaling nature with the experimental parameters is difficult, recently, machine learning has been employed to explore the maximal spreading dynamics [43].

The scaling law being independent of the viscosity of the oil layer can be understood by comparing the viscous dissipation, $\int \mu(\partial u/\partial z)^2 dV$, inside the water drop and the underlying oil layer (Here, dV is the volume element; also see inset of Fig.3). During spreading, the ratio of total viscous dissipation in oil to that in the water can be written as

$$\frac{E_o}{E_w} = \frac{\mu_o(u_o/d_o)^2 d_o \pi R_p^2}{\mu_w((u - u_o)/d_w)^2 d_w \pi R_p^2}, \quad (1)$$

where R_p is the radius of the pancake drop, d_o is the oil

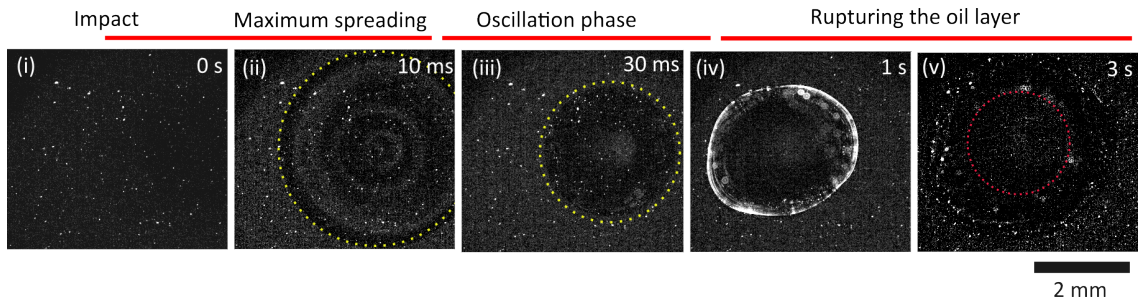


Figure 4. Images showing the impact dynamics of a drop on an oil layer (viscosity: 370 cSt) containing suspended fluorescent particles (diameter $2 \mu\text{m}$). (i)-(ii): From impact to maximum spreading no particles are displaced from their original position, implying the integrity of the oil layer during the drop spreading. (ii)-(iii): Only, a few particles are dragged radially inward during the retraction phase. The yellow dashed circle represents the edge of the water drop. (iv)-(v): From the beginning and end of the rupturing of the oil layer, particles are displaced as the drop penetrated the oil layer. The red dashed circle in (v) represents the oil droplet trapped at the center.

layer thickness, d_w is the pancake drop thickness, u is the fluid velocity at the top of the drop, and u_o is the fluid velocity at the water-oil interface (see inset of Fig.3). At the interface between the water and oil, the viscous stress must balance. Thus, we can write, $\mu_w(u - u_o)/d_w \approx \mu_o u_o/d_o$. Therefore, we can rewrite Eq.1 approximately as

$$\frac{\mu_w}{\mu_o} \frac{d_o}{d_w} \ll 1. \quad (2)$$

Eq.2 implies that the dissipation of the impact energy inside the oil is negligible compared to that in the spreading water drop [41]. Thus, the viscous properties of the underlying oil layer do not play a crucial role in the spreading dynamics. Thus, we can expect the same scaling laws regardless of the oil layer viscosity.

To understand how the initial fast spreading of the water drop displace the oil, we dispersed red fluorescent polystyrene particles of diameter $2 \mu\text{m}$ in the oil (viscosity: 370 cSt). We observed the impact from below the glass slide (Fig.4). Upon impact, the drop spreads without creating any noticeable movement of the particles indicating that the spreading is mostly peripheral. Also the side view of the drop demonstrated an advancing angle more than 90° . After the maximum spread, during the retraction, drop drags the oil radially inward manifested by the corresponding movement of the fluorescent particles. It demonstrates that the drop dissipates its energy in the oil mainly during the retraction phase.

Other effects may also influence the dynamics of impacted drop spreading. For instance, air film entrapment between the impacting drop and the oil layer [24, 44, 45] might cause a differences in the spreading dynamics on the low and high viscous oil surfaces. Since the surface of the relatively low viscous oil deforms faster, a wide air film can be trapped there, which might be minimal with a high viscous oil layer. While the specific mechanisms altering the scaling behavior remain unclear, our

measurements suggest that changes in the viscosity of the impacting surface strongly affect the dynamics of spreading and thus the scaling behaviour.

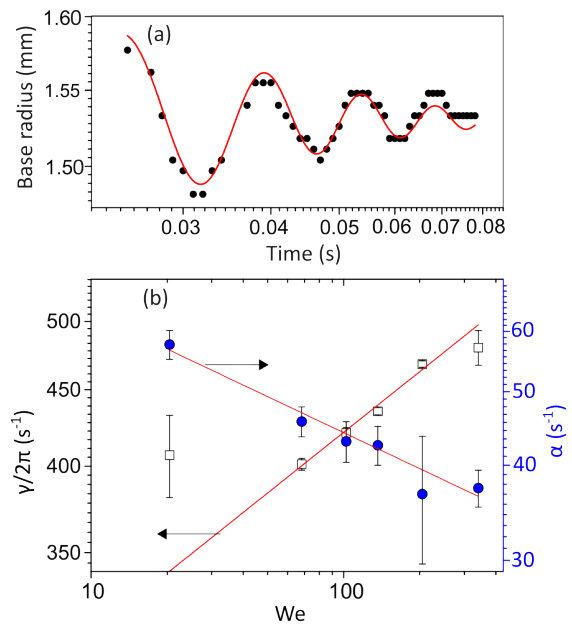


Figure 5. (a) An example of fit of Eq.4 on experimental data of contact line oscillations of a drop impacted from 1 cm height. (b) The fitting parameters, γ and α , as a function of the Weber number. The red lines fitted on γ and α are having slopes of 0.13 ± 0.015 and -0.15 ± 0.013 , respectively.

Drop oscillations: Upon retraction, the drop executes damped oscillations. The oscillatory motion of the contact line can be seen in Fig.2. A simple analogy with the spring-mass system can capture the damped oscillation dynamics of the drop [46]. Therefore, we can write,

$$m\ddot{y} + c\dot{y} + ky = 0, \quad (3)$$

where, m is the mass, y is the displacement, c is the damping coefficient and k is the spring constant. The general solution to Eq.3 is

$$y(t) = Ae^{-\alpha t} \sin(\gamma t + \phi), \quad (4)$$

where $\alpha = c/2m$, $\gamma = \sqrt{\omega^2 - \alpha^2}$, $\omega^2 = k/m$, and $A = y(0)$.

In Fig.3(a), we plotted the frequency γ and the damping factor α , obtained by fitting Eq.4 to the oscillating regions of the curves, as a function of We , i.e, with increasing impact velocity. We see that $\alpha \sim We^{-0.15}$ and $\gamma \sim We^{0.15}$, where the same power with opposite signs is expected as $\gamma = \sqrt{\omega^2 - \alpha^2}$.

An increased degree of damping with increasing We is expected. It is important to note that the retraction phase is responsible for dissipating most of the energy. When the impact velocity is higher, the droplet spreads over a larger area, and the dissipation increases proportionally. Thus, with increasing We , the available energy for oscillations becomes less and the initial amplitude of oscillation decreases. Therefore, the effective decay rate α also decreases with We .

The damping factor is related to the ratio of viscous force to inertia force or the inverse of the Reynolds number. Therefore, in Supplementary Fig.S2, we have plotted the values of α as a function of Re , which indicates a relationship $\alpha \sim Re^{-1/4}$.

A typical damping time can be estimated as $t_{damp} = \rho_w R^2 / \mu_w$, which gives a value of about 1 s with $R \sim 1$ mm. Using the viscosity of oil (μ_o), we estimate a damping time of 1 ms, which is much shorter than the experimentally observed value of about 0.3 s. Thus, we assume that most of the damping occurs within the water drop, also in accordance with Eq.2.

Drop penetration into the oil layer and spreading: Throughout the damping oscillations, both the base radius and the corresponding contact angle maintained a consistent average value for a duration of t_R as evident in Fig.2. For example, the contact angle, constant around approximately 100° , decreases to approximately 35° at around t_R . The corresponding increase in the base radius is also apparent. We observed similar spreading also with PDMS and ITO surfaces coated with oil. When an oil layer ($7 \mu\text{m}$ thick) was applied to PDMS and ITO surfaces, after a duration t_R , the final contact angles were measured to be $100 \pm 2^\circ$ and $65 \pm 2^\circ$, respectively. These values closely align with the contact angles observed on the corresponding bare surfaces, namely $100 \pm 2^\circ$ for PDMS and $60 \pm 2^\circ$ for ITO. These findings strongly suggest that the change in contact angle occurs

as the drop's contact line penetrates the oil layer and interacts with the underlying substrate. This is expected, as the oil density (971 kg/m^3) is slightly lower than that of water.

On glass, the final contact angle did not match the contact angle of water on the bare substrate. For example, while the drop displayed a contact angle of 22° on bare glass, it exhibited a slightly larger angle (approximately 35°) after spreading with an oil layer. This difference might be attributed to the potential presence of a thin oil film trapped beneath the spreading drop [47, 48].

We further looked into the details of the water penetration into the oil layer. The bottom view of the drop shows that, before the water drop spreads over the underlying substrate, the water ruptures the oil layer and the dewetting of the oil layer follows. The rupturing and dewetting process starts only a few hundred microseconds after the impact. This short delay might be due to the entrapped air layer between the drop and the oil as observed in experiments involving water drops being engulfed by the oil with some initial delay due to air entrapment [49].

The dewetting process is shown the images in Fig. 6(a) and Supplementary video 1. The entrapped air and the dewetting process delay penetration of the drop edge into the oil. This overall delay in the drop edge penetration, denoted by t_R , amounts to about one second on 370 cSt oil and over 50 seconds on 10000 cSt oil layers (Fig. 6(b)).

The rupturing and dewetting of the oil is initiated somewhere under the bulk region of the drop (Fig. 6(a) and Supplementary video 1). Under the drop, as the dewetting advances a hole is opened up in the oil layer and the water wets the substrate. Assuming a thin oil layer at the dewetting region, the initial dewetting velocity can be estimated as [50],

$$v_{dw} = \frac{k \sigma_{ow} \theta_E^3}{\mu_o}, \quad (5)$$

where σ_{ow} is the interfacial tension between oil and water, θ_E^3 is the equilibrium contact angle of oil on glass surface, and k is a numerical coefficient that ranges between 10^{-2} and 10^{-3} and related to the molecular properties of the liquid [50]. With $\sigma_{ow} = 39 \text{ mN/m}$ [51], $\theta_E = 87^\circ$, and $k = 10^{-2}$, we calculate a velocity of 3.7 mm/s for the case $\mu_o = 370 \text{ cSt}$. This value is very close to the measured dewetting velocity of $5 \pm 2 \text{ mm/s}$ for oil viscosity 370 cSt. The measured value was about 0.03 mm/s for oil viscosity 10000 cSt.

As shown in Fig. 6(a), eventually, the dewetted oil converges to form a small droplet at the central region under the water drop (Supplementary video 1). This oil droplet formation is driven by the relatively strong interfacial tension of oil/water interface (39 mN/m) [51]. Despite the oil having a slightly lower density, the oil droplet adheres to the substrate without ascending within the water drop.

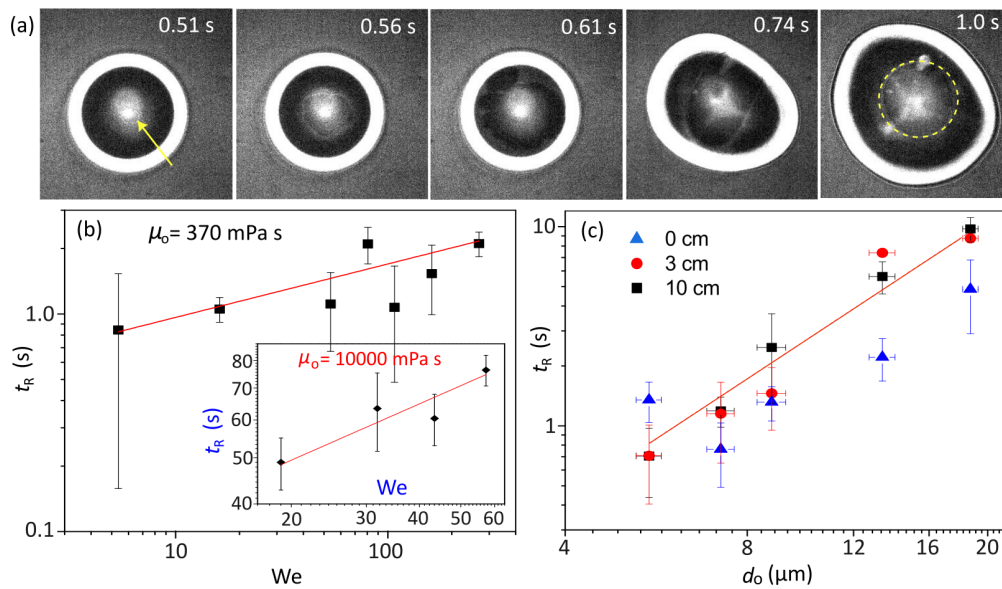


Figure 6. (a) About 0.5 s after impact, water ruptures the oil layer (marked by the arrow) and initiate the dewetting of the oil layer. Finally, under the spreading water drop, an oil droplet is formed (see inside the dashed circle on panel of 1.0 s and Supplementary video 1). The bright circular periphery of the drop is due to light reflection. (b-c) The onset time of drop edge spreading t_R depends on We and d_o . (b) t_R demonstrates an increase with the Weber number, with power approximately as $We^{1/4}$. ($d_o = 7 \mu\text{m}$). (c) We note that t_R shows an increasing trend with the thickness of the oil layer. The red solid line has a slope of 2.0.

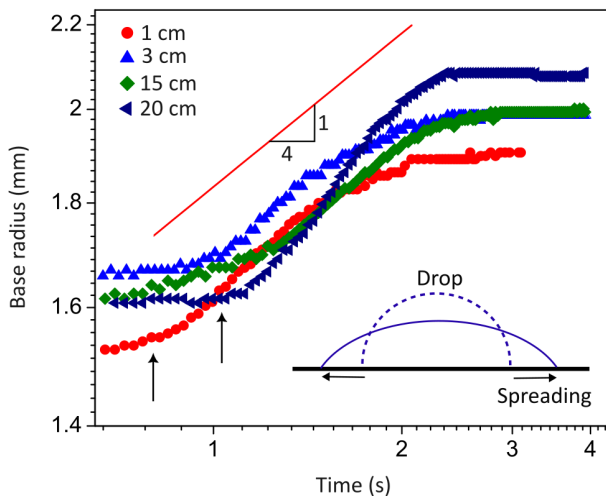


Figure 7. After impact, the drop spreads across the solid surface beneath the oil layer after a duration t_R (marked by the arrows). The base radius R_b follows a scaling relation of $t^{0.25}$. The impact heights are shown in the panel. The schematic in the inset illustrates the initial (dashed line) and final (solid line) shapes of the drop as it spreads.

We observed that only when the dewetted oil converges under the water drop, the edge of the water drop starts to spread outward, i.e., at time t_R . Thus, neglecting the delay (a few hundred microseconds) imparted by the air entrapment, the value of t_R is mainly the time for com-

pletion of the dewetting process, which can be estimated as

$$t_R \sim \frac{R_b}{v_{dw}}, \quad (6)$$

where R_b is the equilibrium base radius of the water drop. With $R_b = 1.6 \text{ mm}$, we obtain t_R as 0.43 s and 11 s for oils of viscosity 370 and 10000 cSt, respectively. The t_R values for the highly viscous oil can be even larger, as the values of k may be smaller than 10^{-2} . Therefore, the estimated values of t_R align closely with the observed ones in our experiments.

We further study the influence of the impact parameters on the delay time t_R . The value of t_R rises with the We , as demonstrated in Fig. 6(b). This observation may seem counter-intuitive, as one might anticipate that a greater impact velocity would expedite the drop's penetration into the oil layer, resulting in an earlier encounter with the underlying substrate. However, the opposite trend suggests that the impacting drop does not promptly displace the oil layer, as was also evident from Fig. 4. We observed that t_R follows a relationship of $t_R \sim We^{0.25 \pm 0.05}$ for oil with viscosity 370 cSt, and $t_R \sim We^{0.4 \pm 0.1}$ for oil with viscosity 10000 cSt, as shown in Fig. 6(b).

Our measurements show that t_R depends upon the oil thickness as well. Remarkably, as illustrated in Fig. 6(c), it follows a power-law relationship, denoted by $t_R \sim d_o^{1.9 \pm 0.2}$. This exponent, exceeding 1.0, implies that

the drop's edge isn't sinking freely. The observed exponent can be related with the dewetting process. When a hole appears on a viscous thin layer of thickness e , the dewetting proceeds until its thickness increases to a value $e_c = 2\kappa^{-1}\sin(\theta_E/2)$, where κ^{-1} is the capillary length [50]. Thus, as the layer thickness increases during the dewetting, the velocity takes the form [50],

$$v_{dw} \sim e_c^2 - e^2, \quad (7)$$

with $e(t) \leq e_c$. Thus, v_{dw} decreases as $e_c^2 - e^2$ with time. An estimated value of t_R can be obtained from the average velocity as $t_R \sim R_b / \langle e_c^2 - e^2 \rangle$. It aligns with the observation that $t_R \sim d_o^2$. The exact expression connecting the temporal variation of v_{dw} and the observed scaling with initial oil layer thickness (d_o) and Weber number may require further theoretical investigations.

Followed by the dewetting, the drop spreads over the substrate surface. It shows an increase in the base radius (see region after about 1 s in Fig. 2(a)). We plotted this region of the curves in Fig. 7. Our findings reveal a scaling behavior of $R_b \sim t^{0.25 \pm 0.07}$. Typically, the initial spreading dynamics of drops conform to a power law. For instance, in the inertial-capillary regime, a scaling law of $R_b \sim t^{0.5}$ has been documented [52, 53]. However, in the viscous-capillary regime, various exponents have been reported [52, 54]. As the viscous drop spreads, the exponent diminishes over time, eventually reaching 1/10 on wetting surfaces [52, 55]. Despite our drop being a low-viscosity liquid (water), the resistance posed by the viscous oil affects the movement of the contact line. Moreover, the spreading regime does not align with early times, as the drop had already partially spread on the oil layer. Consequently, we anticipate a smaller exponent, indicative of the late-time dynamics of viscous droplets, in our case.

DISCUSSION

Our observation that the impacted drop initially does not deform the oil layer contrast with the findings from other studies on water drop impact on oil [31–33]. For instance, Che et al. [31] examined water drop impact on silicone oil layers with viscosities ranging from 5 to 50 cSt. They noted that the impacted drop displaces the oil layer, but this effect diminishes with increasing oil viscosity, consistent with our findings. Our measurements, conducted at much higher viscosity (370 and 10000 cSt), reveal that the impacted drop does not disturb the oil layer during its spreading phase.

While the drops spread on high-viscosity oil almost akin to a solid surface, the retraction phase involves significant viscous dissipation. This could be attributed to the dragging of the oil along with the retracting contact

line. Conversely, in experiments with very low viscosity, such as our trials with 20 cSt silicone oil, the retracted water drop retained considerable kinetic energy, resulting in the formation of a vertically elongated jet shape (see Supplementary Fig. S3). At large impact energies, this jet subsequently broke up to form a small drop at the tip. This observation aligns with previous findings indicating that the bouncing of the impacted drop occurs when the oil viscosity is low [33].

SUMMARY

In our experimental study, we investigated the impact of water drops on thin layers of viscous oil applied to solid surfaces. We observed a series of dynamic phenomena, including maximal spreading and retraction, oscillations, delayed penetration into the oil layer, and spreading on the solid surface. We show that the viscosity of the underlying oil layer does not affect the scaling relationship for the maximum spreading radius ($\beta \sim We^{1/4}$).

Following spreading and retraction, the drop undergoes oscillations, maintaining a constant average base radius and contact angle for a duration t_R (a few seconds). During this time the water slowly ruptures the oil layer and dewets the oil under the drop, eventually converging as a small oil droplet under the spreading water drop. Intriguingly, we observed a nonlinear relationship between t_R and the thickness of the oil layer ($t_R \propto d_o^2$), which we relate to the dewetting dynamics of oil layer under the water drop. Similarly, t_R increases with the Weber number approximately as $We^{1/4}$, indicating a complex interplay between the dewetting process, oil layer thickness, and impact energy. In summary, we unveil previously unreported short-term and long-term dynamics of drops impacting on oil layers. Our findings may inspire new experimental and theoretical investigations in related areas.

ACKNOWLEDGMENT

DM acknowledges IISER Tirupati intramural funds and Science and Engineering Research Board (India) grant CRG/2020/003117.

COMPETING FINANCIAL INTERESTS

The authors declare no competing financial interests.

* dileep.mampallil@iisertirupati.ac.in

- [1] A. Prosperetti and H. N. Oguz, The impact of drops on liquid surfaces and the underwater noise of rain, *Annual Review of Fluid Mechanics* **25**, 577 (1993).
- [2] A. Yarin, Drop impact dynamics: Splashing, spreading, receding, bouncing, *Annual Review of Fluid Mechanics* **38**, 159 (2006).
- [3] C. Josserand and S. Thoroddsen, Drop impact on a solid surface, *Annual Review of Fluid Mechanics* **48**, 365 (2016).
- [4] G. Liang and I. Mudawar, Review of drop impact on heated walls, *International Journal of Heat and Mass Transfer* **106**, 103 (2017).
- [5] C. W. Visser, P. E. Frommhold, S. Wildeman, R. Mettin, D. Lohse, and C. Sun, Dynamics of high-speed micro-drop impact: numerical simulations and experiments at frame-to-frame times below 100 ns, *Soft Matter* **11**, 1708 (2015).
- [6] D. Khojasteh, M. Kazerooni, S. Salarian, and R. Kamali, Droplet impact on superhydrophobic surfaces: A review of recent developments, *Journal of Industrial and Engineering Chemistry* **42**, 1 (2016).
- [7] G. Delon, D. Terwagne, S. Dorbolo, N. Vandewalle, and H. Caps, Impact of liquid droplets on granular media, *Phys. Rev. E* **84**, 046320 (2011).
- [8] M. Sharma, M. Gopu, J. E. George, S. Gupta, and D. Mampallil, Drop impact on thin powder layers: pattern formation by air entrapment, *Soft Matter* **16**, 1342 (2020).
- [9] A. I. Fedorchenko and A.-B. Wang, On some common features of drop impact on liquid surfaces, *Physics of Fluids* **16**, 1349 (2004).
- [10] D. Bonn, J. Eggers, J. Indekeu, J. Meunier, and E. Rolley, Wetting and spreading, *Rev. Mod. Phys.* **81**, 739 (2009).
- [11] G. D. Martin, S. D. Hoath, and I. M. Hutchings, Inkjet printing - the physics of manipulating liquid jets and drops, *Journal of Physics: Conference Series* **105**, 012001 (2008).
- [12] A. T. Chandantaru Dey Modak, Arvind Kumar and P. Sen, Drop impact printing, *Nat Commun* **11**, 4327 (2020).
- [13] C. Park, J. Seol, A. Aldabahi, M. Rahaman, A. L. Yarin, and S. S. Yoon, Drop impact phenomena and spray cooling on hot nanotextured surfaces of various architectures and dynamic wettability, *Physics of Fluids* **35**, 027126 (2023).
- [14] M. Massinon, N. De Cock, W. A. Forster, J. J. Nairn, S. W. McCue, J. A. Zabkiewicz, and F. Lebeau, Spray droplet impaction outcomes for different plant species and spray formulations, *Crop Protection* **99**, 65 (2017).
- [15] F. m. c. Boyer, E. Sandoval-Nava, J. H. Snoeijer, J. F. Dijksman, and D. Lohse, Drop impact of shear thickening liquids, *Phys. Rev. Fluids* **1**, 013901 (2016).
- [16] F. R. Smith, C. Nicloux, and D. Brutin, Influence of the impact energy on the pattern of blood drip stains, *Phys. Rev. Fluids* **3**, 013601 (2018).
- [17] D. P. Attinger, C. Moore, A. Donaldson, A. Jafari, and H. A. Stone, Fluid dynamics topics in bloodstain pattern analysis: comparative review and research opportunities., *Forensic Sci Int.* **231**, 375 (2013).
- [18] C. Clanet, C. Beguin, D. Richard, and D. Quere, Maximal deformation of an impacting drop, *Journal of Fluid Mechanics* **517**, 199–208 (2004).
- [19] J. B. Lee, D. Derome, A. Dolatabadi, and J. Carmeliet, Energy budget of liquid drop impact at maximum spreading: Numerical simulations and experiments, *Langmuir* **32**, 1279 (2016), pMID: 26745364.
- [20] Y. C. Jung and B. Bhushan, Dynamic effects of bouncing water droplets on superhydrophobic surfaces, *Langmuir* **24**, 6262 (2008).
- [21] J. C. Bird, R. Dhiman, H.-M. Kwon, and K. K. Varanasi, Reducing the contact time of a bouncing drop, *Nature* **503**, 385–388 (2013).
- [22] Z. Hu, F. Chu, Y. Lin, and X. Wu, Contact time of droplet impact on inclined ridged superhydrophobic surfaces, *Langmuir* **38**, 1540 (2022), pMID: 35072484.
- [23] J. de Ruiter, D. Soto, and K. Varanasi, Self-peeling of impacting droplets., *Nature Phys* **14**, 35 (2018).
- [24] J. de Ruiter, J. M. Oh, D. van den Ende, and F. Mugele, Dynamics of collapse of air films in drop impact, *Phys. Rev. Lett.* **108**, 074505 (2012).
- [25] H. Katsuragi and J. Blum, Impact-induced energy transfer and dissipation in granular clusters under microgravity conditions, *Phys. Rev. Lett.* **121**, 208001 (2018).
- [26] H. Katsuragi, Length and time scales of a liquid drop impact and penetration into a granular layer, *Journal of Fluid Mechanics* **675**, 552–573 (2011).
- [27] Q. Zhang, M. Gao, R. Zhao, and X. Cheng, Scaling of liquid-drop impact craters in wet granular media, *Phys. Rev. E* **92**, 042205 (2015).
- [28] R. Rioboo, M. Voué, H. Adão, J. Conti, A. Vaillant, D. Seveno, and J. De Coninck, Drop impact on soft surfaces: Beyond the static contact angles, *Langmuir* **26**, 4873 (2010).
- [29] L. Chen, E. Bonaccorso, P. Deng, and H. Zhang, Droplet impact on soft viscoelastic surfaces, *Phys. Rev. E* **94**, 063117 (2016).
- [30] A. Alizadeh, V. Bahadur, W. Shang, Y. Zhu, D. Buckley, A. Dhinojwala, and M. Sohal, Influence of substrate elasticity on droplet impact dynamics, *Langmuir* **29**, 4520 (2013).
- [31] Z. Che and O. K. Matar, Impact of droplets on immiscible liquid films, *Soft Matter* **14**, 1540 (2018).
- [32] C. Lee, H. Kim, and Y. Nam, Drop impact dynamics on oil-infused nanostructured surfaces, *Langmuir* **30**, 8400 (2014).
- [33] J.-H. Kim and J. P. Rothstein, Droplet impact dynamics on lubricant-infused superhydrophobic surfaces: The role of viscosity ratio, *Langmuir* **32**, 10166 (2016).
- [34] M. Muschi, B. Brudieu, J. Teisseire, and A. Sauret, Drop impact dynamics on slippery liquid-infused porous surfaces: influence of oil thickness, *Soft Matter* **14**, 1100 (2018).
- [35] D. Meyerhofer, Characteristics of resist films produced by spinning, *Journal of Applied Physics* **49**, 3993 (2008).
- [36] M. Pasandideh-Fard, Y. M. Qiao, S. Chandra, and J. Mostaghimi, Capillary effects during droplet impact on a solid surface, *Physics of Fluids* **8**, 650 (1996).
- [37] J. Eggers, M. A. Fontelos, C. Josserand, and S. Zaleski, Drop dynamics after impact on a solid wall: Theory and simulations, *Physics of Fluids* **22**, 062101 (2010).
- [38] C. Ukiwe and D. Y. Kwok, On the maximum spreading diameter of impacting droplets on well-prepared solid surfaces, *Langmuir* **21**, 666 (2005).
- [39] M. Wörner, Maximum spreading of an impacting drop, *International Journal of Multiphase Flow* **167**, 104528 (2023).
- [40] N. Laan, K. G. de Bruin, D. Bartolo, C. Josserand, and D. Bonn, Maximum diameter of impacting liquid

- droplets, *Phys. Rev. Appl.* **2**, 044018 (2014).
- [41] S. Bandyopadhyay, C. Bakli, R. Mukherjee, and S. Chakraborty, Damped oscillatory dynamics of a drop impacting over oil-infused slippery interfaces-does the oil viscosity slow it down?, *Langmuir* **39**, 12826 (2023).
- [42] J. B. Lee, N. Laan, K. G. de Bruin, G. Skantzaris, N. Shahidzadeh, D. Derome, J. Carmeliet, and D. Bonn, Universal rescaling of drop impact on smooth and rough surfaces, *Journal of Fluid Mechanics* **786**, R4 (2016).
- [43] L. Au-Yeung and P. A. Tsai, Predicting impact outcomes and maximum spreading of drop impact on heated nanostructures using machine learning, *Langmuir* **39**, 18327 (2023).
- [44] W. Bouwhuis, R. C. A. van der Veen, T. Tran, D. L. Keij, K. G. Winkels, I. R. Peters, D. van der Meer, C. Sun, J. H. Snoeijer, and D. Lohse, Maximal air bubble entrainment at liquid-drop impact, *Phys. Rev. Lett.* **109**, 264501 (2012).
- [45] T. Tran, H. de Maleprade, C. Sun, and D. Lohse, Air entrainment during impact of droplets on liquid surfaces, *Journal of Fluid Mechanics* **726**, R3 (2013).
- [46] R. M. Manglik, M. A. Jog, S. K. Gande, and V. Ravi, Damped harmonic system modeling of post-impact drop-spread dynamics on a hydrophobic surface, *Physics of Fluids* **25**, 082112 (2013).
- [47] A. Staicu and F. Mugele, Electrowetting-induced oil film entrapment and instability, *Phys. Rev. Lett.* **97**, 167801 (2006).
- [48] J. Hong, Y. K. Kim, K. H. Kang, J. Kim, and S. J. Lee, Spreading dynamics and oil film entrapment of sessile drops submerged in oil driven by dc electrowetting, *Sensors and Actuators B: Chemical* **196**, 292 (2014).
- [49] C. Cuttle, A. B. Thompson, D. Pihler-Puzović, and A. Juel, The engulfment of aqueous droplets on perfectly wetting oil layers, *Journal of Fluid Mechanics* **915**, A66 (2021).
- [50] D. Q. Pierre-Gilles Gennes, Françoise Brochard-Wyart, *Capillarity and wetting phenomena*, Chapter 7 (2004).
- [51] F. Peters and D. Arabali, Interfacial tension between oil and water measured with a modified contour method, *Colloids and Surfaces A: Physicochemical and Engineering Aspects* **426**, 1 (2013).
- [52] A. Eddi, K. G. Winkels, and J. H. Snoeijer, Short time dynamics of viscous drop spreading, *Physics of Fluids* **25**, 013102 (2013).
- [53] J. Du, N. T. Chamakos, A. G. Papathanasiou, and Q. Min, Initial spreading dynamics of a liquid droplet: The effects of wettability, liquid properties, and substrate topography, *Physics of Fluids* **33**, 042118 (2021).
- [54] S. P. Thampi, I. Pagonabarraga, R. Adhikari, and R. Govindarajan, Universal evolution of a viscous-capillary spreading drop, *Soft Matter* **12**, 6073 (2016).
- [55] L. H. Tanner, The spreading of silicone oil drops on horizontal surfaces, *Journal of Physics D: Applied Physics* **12**, 1473 (1979).